

RESEARCH PAPER



## Synthesis, computational study and biological evaluation of 9-acridinyl and 1-coumarinyl-1,2,3-triazole-4-yl derivatives as topoisomerase II inhibitors

Gehan A. Abdel-Hafez<sup>a</sup>, Abdel-Maaboud I. Mohamed<sup>b</sup>, Adel F. Youssef<sup>c</sup>, Claire Simons<sup>d</sup> and Ahmed S. Aboraia<sup>c</sup>

<sup>a</sup>South Egypt Cancer Institute, Assiut, Egypt; <sup>b</sup>Pharmaceutical Analytical Chemistry Department, Faculty of Pharmacy, Assiut University, Assiut, Egypt; <sup>c</sup>Medicinal Chemistry Department, Faculty of Pharmacy, Assiut University, Assiut, Egypt; <sup>d</sup>School of Pharmacy and Pharmaceutical Sciences, Cardiff University, Cardiff, UK

### ABSTRACT

Topoisomerase (IIB) inhibitors have been involved in the therapies of tumour progression and have become a major focus for the development of anticancer agents. New three-component hybridised ligands, 1,4-disubstituted-1,2,3-triazoles (**8–17**), were synthesised via a 1,3-dipolar cycloaddition reaction of 9-azidoacridine/3-azidocoumarin with N/O-propargyl small molecules under click reaction conditions. Cancer cell growth inhibition of the synthesised triazoles was tested against human cell-lines in the NCI-60-cell-panel, and the most active compounds tested against topoisomerase (IIB)-enzymes. The acridinyl ligands (**8–10**) revealed 60–97% cell growth inhibition in six cancer cell-panels. Cell-cycle analysis of MCF7 and DU-145 cells treated with the active acridinyl ligands exhibited cell-cycle arrest at G2/M phase and proapoptotic activity. In addition, compound **8** displayed greater inhibitory activity against topoisomerase (IIB) (IC<sub>50</sub> 0.52 μM) compared with doxorubicin (IC<sub>50</sub> 0.83 μM). Molecular dynamics simulation studies showed the acridine-triazole-pyrimidine hybrid pharmacophore was optimal with respect to protein-ligand interaction and fit within the binding site, with optimal orientation to allow for intercalation with the DNA bases (DG13, DC14, and DT9).

### ARTICLE HISTORY

Received 19 October 2021  
Revised 13 December 2021  
Accepted 16 December 2021

### KEYWORDS

9-azidoacridine; 3-azidocoumarin; 1,2,3-triazole; topoisomerase IIB inhibitor; molecular dynamics

### Introduction

Second to cardiovascular diseases, cancer is the most common cause of death<sup>1,2</sup>. The urgent need to combat cancer, necessitates developing more effective anticancer agents. Molecular hybridisation in drug design is based on the combination of pharmacophoric moieties of bioactive molecules to produce a new hybrid compound with better activity in comparison compared with the parent compounds. Practice of this technique has afforded bioactive compounds with improved efficacy relative to the component individual subunits<sup>3</sup>.


The ability of the tricyclic planar aromatic structure of acridine to intercalate in the double-stranded DNA structure and the acridine nitrogen adoption of an acceptor or donor conformation, which has a radical effect on the binding properties of the molecule are the major considerations for the use of acridines as anticancer compounds<sup>4,5</sup>. In addition, acridine derivatives prevent abnormal functioning of tumour cells, which includes dysfunction of the enzymes that control the topology of DNA<sup>6</sup>. Topoisomerase, telomerase, and cyclin-dependent kinases (CDKs) are illustrative examples of enzymes inhibited by acridine derivatives such as amsacrine<sup>7</sup>, *N*-[2-(dimethylamino)ethyl]acridine-4-carboxamide (DACA)<sup>8</sup>, and 3-aminoacridine-9(10*H*)-thione (3-ATA) (Figure 1)<sup>9,10</sup>.

On the other hand, coumarins are widely available in plants<sup>11</sup> and exert anticancer activity through various mechanisms including inhibition of telomerase<sup>12</sup>, protein kinase, and by controlling

oncogene expression, or by inducing caspase-9-mediated apoptosis<sup>13</sup>. In addition, researchers have shown that coumarins can suppress the proliferation of cancer cells by stopping the cell cycle<sup>13</sup>. The triazole nucleus is present in an array of drug categories such as antimicrobials, anti-inflammatory, analgesics, and anti-epileptics as a key structural component<sup>14,15</sup>.

In this study, three component ligands were built with a 1,2,3-triazole ring bridging acridine/coumarin nuclei to heteroaryl/aryl/alkyl pharmacologically active molecules (Figure 2). The coumarin and acridine moieties were ligated, via the triazole ring, to different heterocycles to generate the hybrid molecules. Uracil and 6-Me-uracil were chosen owing to the ability of these pyrimidines to form crosslinks with the DNA duplex. Uracil itself is a reversible dihydropyrimidine dehydrogenase (DPD) inhibitor, which has been shown to be beneficial in reducing drug toxicity of other uracil anticancer agents, for example, 5-fluorouracil, tegafur, and capecitabine<sup>16,17</sup> and therefore, may have additional protective properties. Phenytoin, used clinically in the treatment of epilepsy, has multiple modes of action<sup>18</sup> with promising results in studies against breast cancer<sup>19</sup> and phenytoin has also been shown to have cardioprotective effects on doxorubicin-induced cardiotoxicity<sup>20</sup>. Valproic acid, used clinically in the treatment of seizures, has been shown to be an inhibitor of histone deacetylases resulting in anticancer activity<sup>21,22</sup>, while the non-steroidal anti-inflammatory drug (NSAID) naproxen has been shown to display anticancer activity either directly or indirectly through inhibition of COX-2

**CONTACT** Ahmed S. Aboraia  [ahmed.mohamed15@pharm.au.edu.eg](mailto:ahmed.mohamed15@pharm.au.edu.eg)  Medicinal Chemistry Department, Faculty of Pharmacy, Assiut University, Assiut 71526, Egypt

 Supplemental data for this article can be accessed [here](#).

© 2022 The Author(s). Published by Informa UK Limited, trading as Taylor & Francis Group.

This is an Open Access article distributed under the terms of the Creative Commons Attribution-NonCommercial License (<http://creativecommons.org/licenses/by-nc/4.0/>), which permits unrestricted non-commercial use, distribution, and reproduction in any medium, provided the original work is properly cited.

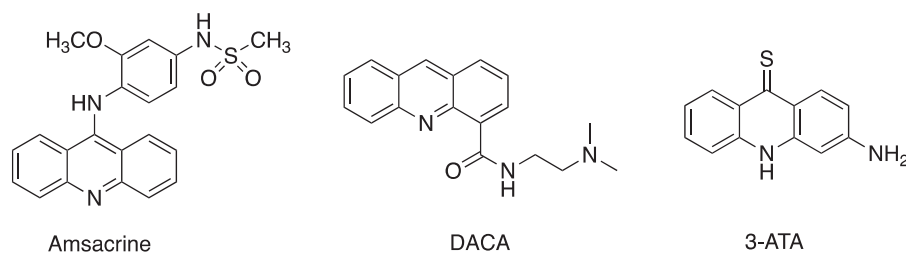


Figure 1. Examples of acridine compounds with anticancer activity.

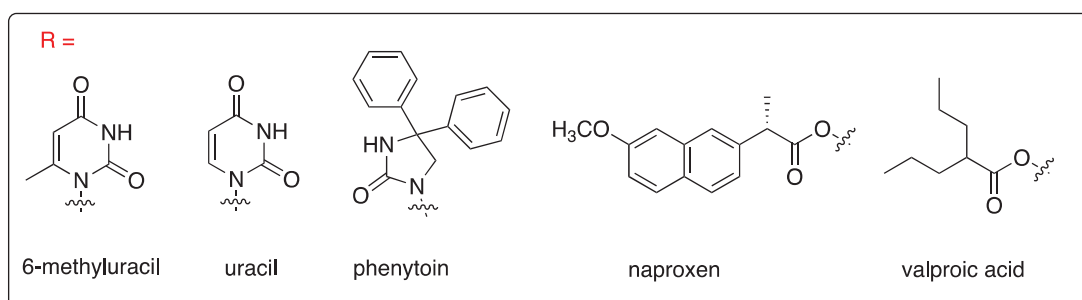
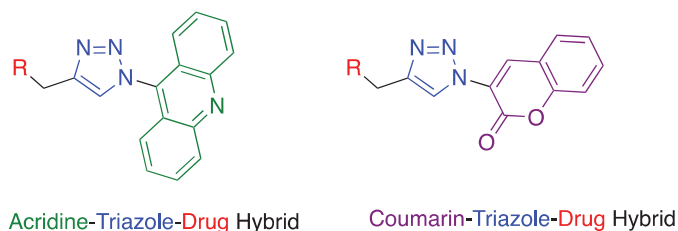


Figure 2. Designed acridine-triazole-drug and coumarin-triazole-drug hybrid compounds.

and several kinases, including PI3K, have been implicated in the anticancer mechanism of action resulting in the induction of cell-cycle arrest and apoptosis<sup>23,24</sup>.

The triazole core mimics an amidic bond and is planar with hydrogen bond donor and acceptor properties; however, in contrast to the amidic bond triazoles are metabolically stable<sup>25</sup>. Moreover, the hydrogen bonding properties of the triazole ring enable formation of C-H... $\pi$  interactions with the respective enzyme or receptor target<sup>26</sup>. The physicochemical properties and pharmacological potential of the 1,4-disubstituted triazole ring combined with the conformational flexibility of the designed ligands are favourable properties in the design of novel bio-active compounds.

## Experimental

### Chemistry

All the chemicals used for the synthesis of the target compounds were of commercially available analytical grade. TLC was carried out using silica gel 60 F<sub>254</sub> pre-coated sheets 20 × 20 cm, layer thickness 0.2 mm (E. Merck, Darmstadt, Germany), and spots were visualised using UV-lamp at  $\lambda_{\max}$  254 nm. Column chromatography was performed using Fluka silica gel 60 (particle size 0.063–0.02 mm). Melting points were measured using an electrothermal apparatus (Stuart Scientific, Redhill, UK), and were uncorrected. Infra-red spectra were determined as KBr disks using a Thermo Scientific Nicolet 6700 FT-IR spectrophotometer (Thermo Fisher Scientific, Waltham, MA) at the Pharmaceutical Service Laboratory, Faculty of Pharmacy, Assiut University, Assiut, Egypt. <sup>1</sup>H NMR and <sup>13</sup>C NMR spectra were performed on a Bruker

Spectrophotometer (Billerica, MA) operating at 400 MHz and 100 MHz, respectively. Chemical shifts are expressed in  $\delta$  values (ppm) relative to tetramethylsilane (TMS) as an internal standard and CDCl<sub>3</sub> and DMSO-d<sub>6</sub> were used as solvents. D<sub>2</sub>O was used for the detection of exchangeable protons. Elemental microanalyses were conducted at the Regional Center for Mycology and Biotechnology, Al-Azhar University, Cairo, Egypt. 6-Methyluracil and propargyl bromide (80% w/v in toluene) were obtained from Sigma Aldrich Co. (Darmstadt, Germany). Preparation and analytical data of compounds **1–2** were as reported<sup>27–31</sup> and **3–7** also as reported<sup>32–35</sup>.

**General synthesis of 1,4-disubstituted-1,2,3-triazoles** – In a mixture of water and *t*-butanol (10 ml, 1:1 v/v), the respective azides (**1–2**) (1 mmol) and propargyl derivatives (**3–7**) (1 mmol) were suspended. Sodium ascorbate (0.1 mmol) was added then a solution of copper (II) sulphate pentahydrate (0.01 mmol, 100  $\mu$ L water). The mixture was heated at 80 °C overnight. The precipitate produced was collected by vacuum filtration, washed with water, dried at 50 °C and purified by column chromatography (EtOAc:hexane, 2:3 v/v).

### 1-((1-(Acridin-9-yl)-1H-1,2,3-triazol-4-yl)methyl)-6-methylpyrimidine-2,4(1H,3H)-dione (**8**)

White solid, yield: 57% (200 mg); mp: 247–250 °C. FT-IR (KBr, cm<sup>-1</sup>): 3181, 3162, 3005, 1715, and 1682. <sup>1</sup>H NMR (DMSO-d<sub>6</sub>)  $\delta$ : 11.3 (1H, s, NH, exchangeable), 8.86 (1H, s, H5-triazole), 8.34 (2H, d, *J*=8.7 Hz, H4, H5-acridine), 7.98 (2H, t, *J*=7.6 Hz, H3, H6-acridine), 7.74 (2H, t, *J*=7.6 Hz, H2, H7-acridine), 7.37 (2H, d, *J*=8.7 Hz, H1, H8-acridine), 5.62 (1H, s, CH-methyluracil), 5.29 (2H, s, CH<sub>2</sub>), 3.33 (3H, s, CH<sub>3</sub>). <sup>13</sup>C NMR (DMSO-d<sub>6</sub>)  $\delta$ : 163.05, 154.72, 152.06, 149.12,

143.9, 137.84, 131.71, 129.82, 129.05, 128.29, 122.76, 122.09, 101.88, 40.62, and 20.08. Elemental analyses: found: C%, 65.78; H%, 4.27; N%, 22.09. Calc for  $C_{21}H_{16}N_6O_2$  (MW 384.39): C%, 65.62; H%, 4.20; N%, 21.86. MS calculated for  $C_{21}H_{16}N_6O_2$  (M+): 384.39; found: 384.08.

**1-((1-(Acridin-9-yl)-1H-1,2,3-triazol-4-yl)methyl)pyrimidine-2,4(1H,3H)-dione (9)**

White solid, yield: 61% (200 mg); mp: 254–256 °C. FT-IR (KBr,  $cm^{-1}$ ): 3183, 3155, 3049, 1705, 1682, and 1630.  $^1H$  NMR (DMSO- $d_6$ )  $\delta$ : 11.38 (1H, s, NH, exchangeable), 8.87 (1H, s, H5-triazole), 8.34 (2H, d,  $J=8.7$  Hz, H4, H5-acridine), 7.98 (2H, t,  $J=7.6$  Hz, H3, H6-acridine), 7.94 (1H, d,  $J=7.9$  Hz, H6-uracil), 7.72 (2H, t,  $J=7.6$  Hz, H2, H7-acridine), 7.38 (2H, d,  $J=8.7$  Hz, H1, H8-acridine), 5.68 (1H, d,  $J=7.8$  Hz, H5-uracil), and 5.22 (2H, s,  $CH_2$ ).  $^{13}C$  NMR (DMSO- $d_6$ )  $\delta$ : 164.26, 151.38, 149.12, 146.13, 143.73, 137.82, 131.71, 129.83, 129.03, 128.40, 122.75, 122.06, 101.95, and 42.96. Elemental analyses, found: C%, 65.02; H%, 3.85; N%, 22.93. Calc for  $C_{20}H_{14}N_6O_2$  (MW 370.37): C%, 64.86; H%, 3.81; N%, 22.69.

**3-((1-(Acridin-9-yl)-1H-1,2,3-triazol-4-yl)methyl)-5,5-diphenylimidazolidine-2,4-dione (10)**

Yellow solid, yield: 80% (370 mg); mp: 263–265 °C. FT-IR (KBr,  $cm^{-1}$ ): 3213, 3160, 3108, 1770, 1709, and 1628.  $^1H$  NMR (DMSO- $d_6$ )  $\delta$ : 9.79 (1H, s, NH, exchangeable), 8.84 (1H, s, H5-triazole), 8.33 (2H, d,  $J=8.7$  Hz, H4, H5-acridine), 7.97 (2H, t,  $J=7.6$  Hz, H3, H6-acridine), 7.68 (2H, t,  $J=7.6$  Hz, H2, H7-acridine), 7.38 (10H, m, H-phenyl), 7.29 (2H, d,  $J=8.7$  Hz, H1, H8-acridine), and 5.00 (2H, s,  $CH_2$ ).  $^{13}C$  NMR (DMSO- $d_6$ )  $\delta$ : 173.4, 155.33, 149.11, 143.02, 140.03, 137.82, 131.68, 129.84, 129.04, 128.97, 128.72, 128.37, 127.26, 122.56, 122.10, 69.84, and 40.63. Elemental analyses, found: C%, 73.12; H%, 4.41; N%, 16.70. Calc for  $C_{31}H_{22}N_6O_2$  (MW 510.55): C%, 72.93; H%, 4.34; N%, 16.46.

**1-((1-(Acridin-9-yl)-1H-1,2,3-triazol-4-yl)methyl(2S)-2-(6-methoxynaphthalen-2-yl)propanoate (11)**

General procedure was followed with the exception of heating at 50 °C. White solid, yield: 45% (200 mg); mp: 138–140 °C. FT-IR (KBr,  $cm^{-1}$ ): 3184, 3058, 1705, and 1682.  $^1H$  NMR (DMSO- $d_6$ )  $\delta$ : 8.72 (1H, s, H5-triazole), 8.33 (2H, d,  $J=8.7$  Hz, H4, H5-acridine), 7.96 (2H, t,  $J=7.6$  Hz, H3, H6-acridine), 7.74 (3H, d,  $J=9.3$  Hz, H-naphth), 7.63 (2H, t,  $J=7.6$  Hz, H2, H7-acridine), 7.42 (H, d,  $J=8.4$  Hz, H-naphth), 7.24 (3H, d,  $J=9$  Hz, H-naphth, H1, H8-acridine), 7.08 (1H, dd,  $J=1.8$  Hz, 8.9 Hz, H-naphth.), 5.45 (2H, s,  $CH_2$ ), 4.05 (1H, q,  $J=7$  Hz,  $CHCH_3$ ), 3.85 (3H, s,  $OCH_3$ ), and 1.53 (3H, d,  $J=7$  Hz,  $CHCH_3$ ).  $^{13}C$  NMR (DMSO- $d_6$ )  $\delta$ : 174.13, 157.66, 149.09, 143.73, 137.64, 135.87, 133.77, 131.67, 129.83, 129.55, 129.29, 128.98, 128.82, 127.43, 126.63, 126.15, 122.52, 121.99, 119.20, 106.13, 57.77, 55.63, 44.81, and 18.86. Elemental analyses, found: C%, 73.90; H%, 4.98; N%, 11.67. Calc for  $C_{30}H_{24}N_4O_3$  (MW 488.54): C%, 73.76; H%, 4.95; N%, 11.47.

**1-((1-(Acridin-9-yl)-1H-1,2,3-triazol-4-yl)methyl valproate (12)**

To a solution of 9-azidoacridine **1** (150 mg, 0.68 mmol) in THF (8 ml) and propargyl valproate **9** (370 mg, 2 mmol), sodium ascorbate (13.5 mg, 0.067 mmol) was added then copper (II) sulphate pentahydrate aqueous solution (1.7 mg, 0.0068 mmol, in water 100  $\mu$ L). The mixture was heated at 60 °C with vigorous stirring overnight. The reaction mixture was diluted with water (20 ml), extracted with EtOAc (30 ml (and dried ( $Na_2SO_4$ )). The organic layer

was evaporated and the residue purified by column chromatography (hexane:EtOAc 3:2 v/v) to give the product as a yellow crystalline solid, yield: 46% (125 mg), mp 100–102 °C. FT-IR (KBr,  $cm^{-1}$ ): 3108, 3068, 2858, 1731, and 1629.  $^1H$  NMR ( $CDCl_3$ )  $\delta$ : 8.43 (2H, d,  $J=8.7$  Hz, H4, H5-acridine), 8.14 (1H, s, H5-triazole), 7.90 (2H, t,  $J=7.7$  Hz, H3, H6-acridine), 7.61 (2H, t,  $J=7.6$  Hz, H2, H7-acridine), 7.46 (2H, d,  $J=8.7$  Hz, H1, H8-acridine), 5.50 (2H, s,  $CH_2$ ), 2.49 (1H, m, CH), 1.65 (2H, m,  $CH_2$ ), 1.47 (2H, m,  $CH_2$ ), 1.30 (4H, m,  $2CH_2$ ), and 0.92 (6H, t,  $2CH_3$ ,  $J$  7.3).  $^{13}C$  NMR ( $CDCl_3$ )  $\delta$ : 176.54, 148.39, 143.81, 138.06, 131.50, 128.99, 128.49, 127.97, 122.28, 122.16, 57.08, 45.14, 34.65, 20.66, and 13.96. Elemental analyses, found: C%, 71.42; H%, 6.59; N%, 14.15. Calc for  $C_{24}H_{26}N_4O_2$  (MW 402.49): C%, 71.62; H%, 6.51; N%, 13.92.

**6-Methyl-1-((1-(2-oxo-2H-chromen-3-yl)-1H-1,2,3-triazol-4-yl)methyl)pyrimidine-2,4(1H,3H)-dione(13)**

White solid, yield: 74% (250 mg); mp: 279–283 °C. FT-IR (KBr,  $cm^{-1}$ ): 3182 (NH), 3165, 3025, 2784, 1728, 1714, and 1697.  $^1H$  NMR (DMSO- $d_6$ ) 11.3 (1H, s, NH exchangeable), 8.71 (1H, s, H-triazole), 8.57 (1H, s, C=CH), 7.93(1H, d,  $J=7$ , H8), 7.76–7.71 (1H, ddd,  $J=7.82$  Hz, 7.8 Hz, 1.12 Hz, H7), 7.55 (1H, d,  $J=8.3$  Hz, H6), 7.49–7.45 (1H, t,  $J=7.5$  Hz, H5), 5.56 (1H, s, H5-uracil), 5.14 (2H, s,  $CH_2$ ), and 2.40 (3H, s,  $CH_3$ ).  $^{13}C$  NMR (DMSO- $d_6$ )  $\delta$ : 163, 156.35, 154.63, 152.91, 151.98, 143.44, 135.59, 133.46, 129.99, 125.82, 125.06, 123.61, 118.57, 116.75, 101.75, 40.52, and 19.93. Elemental analyses, found: C%, 58.34; H%, 3.70; N%, 20.12. Calc for  $C_{17}H_{13}N_5O_4$  (MW 351.32): C%, 58.12; H%, 3.73; N%, 19.93.

**1-((1-(2-Oxo-2H-chromen-3-yl)-1H-1,2,3-triazol-4-yl)methyl)pyrimidine-2,4(1H,3H)-dione (14)**

White solid, yield: 62% (200 mg); mp: 262–264 °C. FT-IR (KBr,  $cm^{-1}$ ): 3282, 3185, 3045, 1715, 1700, and 1627.  $^1H$  NMR (DMSO- $d_6$ )  $\delta$ : 11.35 (1H, s, NH, exchangeable), 8.73 (1H, s, H5-triazole), 8.63 (1H, s, C=CH), 7.95–7.93 (1H, dd,  $J=7.7$  Hz, 1.08, H8), 7.84 (1H, d,  $J=7.8$  Hz, H6-uracil), 7.74 (1H, ddd,  $J=7.85$  Hz, 7.8 Hz, 1.4 Hz, H7), 7.55 (1H, d,  $J=8.3$  Hz, H6), 7.47 (1H, t,  $J=7.5$  Hz, H5), 5.63 (1H, dd,  $J=7.8$  Hz, 2.08 Hz, H5-uracil), and 5.07 (2H, s,  $CH_2$ ).  $^{13}C$  NMR (DMSO- $d_6$ )  $\delta$ : 164.18, 156.33, 152.91, 151.98, 145.99, 143.20, 135.46, 133.44, 130, 125.82, 125.12, 123.61, 118.61, 116.75, 101.83, and 42.75. Elemental analyses, found: C%, 57.16; H%, 3.31; N%, 20.89. Calc for  $C_{16}H_{11}N_5O_4$  (MW 337.29): C%, 56.98; H%, 3.29; N%, 20.76.

**3-((1-(2-Oxo-2H-chromen-3-yl)-1H-1,2,3-triazol-4-yl)methyl)-5,5-diphenylimidazolidine-2,4-dione (15)**

White solid, yield: 50% (230 mg); mp: 238–240 °C. FT-IR (KBr,  $cm^{-1}$ ): 3339, 1760, 1733, 1710, and 1653.  $^1H$  NMR (DMSO- $d_6$ )  $\delta$ : 9.75 (1H, s, NH, exchangeable), 8.73 (1H, s, H5-triazole), 8.56 (1H, s, C=CH), 7.93 (1H, d,  $J=7.7$  Hz, H8), 7.73 (1H, ddd,  $J=11.4$  Hz, 7.28 Hz, 1 Hz, H7), 7.55 (1H, d,  $J=8.3$  Hz, H6), 7.47 (1H, t,  $J=7.5$  Hz, H5), 7.42–7.33 (10H, m, H-phenyl), and 4.84 (2H, s,  $CH_2$ ).  $^{13}C$  NMR (DMSO- $d_6$ )  $\delta$ : 173.36, 156.33, 155.29, 152.88, 142.77, 139.97, 135.18, 133.37, 129.97, 129.10–128.71, 127.29, 126.92, 125.79, 124.56, 124.09, 123.63, 118.63, 116.73, 69.84, and 51.02. Elemental analyses, found: C%, 68.11; H%, 4.08; N%, 14.86. Calc for  $C_{27}H_{19}N_5O_4$  (MW 477.47): C%, 67.92; H%, 4.01; N%, 14.67.

### 1-(1-(2-Oxo-2H-chromen-3-yl)-1H-1,2,3-triazol-4-yl)methyl-(S)-2-(6-methoxynaphthalen-2-yl)propanoate (16)

White solid, yield: 46% (200 mg); mp: 142–144 °C. FT-IR (KBr,  $\text{cm}^{-1}$ ): 3182, 1730, 1716, and 1609.  $^1\text{H}$  NMR ( $\text{DMSO-d}_6$ ) 8.70 (1H, s, H5-triazole), 8.56 (1H, s, C=CH), 7.93 (1H, dd,  $J=7.18$  Hz, 0.08 Hz, H8), 7.74 (4H, m, H7, 3H-naphth), 7.55 (1H, d,  $J=8.3$  Hz, H6), 7.48 (1H, ddd,  $J=0.8$  Hz, 7.7 Hz, 7.5 Hz, H5), 7.39 (1H, dd,  $J=8.4$  Hz, 1.6 Hz, H2-naphth.), 7.27 (1H, d,  $J=2.3$  Hz, H3-naphth), 5.32 (2H, dd,  $J=12$  Hz, 21 Hz,  $\text{CH}_2$ ), 3.98 (1H, q,  $J=7$ ,  $\text{CHCH}_3$ ), 3.84 (3H, s,  $\text{OCH}_3$ ), and 1.49 (3H, d,  $J=7.12$  Hz,  $\text{CH-CH}_3$ ).  $^{13}\text{C}$  NMR ( $\text{DMSO-d}_6$ )  $\delta$ : 174.17, 157.66, 156.27, 152.90 (C), 142.66, 135.89, 135.37, 133.79, 133.42, 129.99, 129.60, 128.82, 127.50, 126.69, 126.10, 126.06, 125.80, 123.50, 119.21, 118.61, 116.75, 106.15 (CH), 57.76, 55.61, 44.76 (CH), and 18.97 ( $\text{CH}_3$ ). Elemental analyses, found: C%, 68.78; H%, 4.73; N%, 9.40. Calc for  $\text{C}_{26}\text{H}_{21}\text{N}_3\text{O}_5$  (MW 455.46): C%, 68.56; H%, 4.65; N%, 9.23.

### 1-(2-Oxo-2H-chromen-3-yl)-1H-1,2,3-triazol-4-yl)methyl valproate (17)

3-Azido-2H-chromen-2-one **2** (150 mg, 0.8 mmol) and propargyl valproate **7** (440 mg, 2.4 mmol) were dissolved in THF (8 ml). Sodium ascorbate (20 mg, 0.1 mmol) was added then copper (II) sulphate pentahydrate solution (2 mg, 0.008 mmol, in  $\text{H}_2\text{O}$  100  $\mu\text{L}$ ). The mixture was heated at 60 °C and stirred vigorously overnight. The reaction mixture was diluted with water (20 ml), extracted with EtOAc (30 ml (and dried  $\text{Na}_2\text{SO}_4$ ). The organic layer was evaporated and the residues purified by column chromatography (hexane:EtOAc 3:2 v/v) to give the product as yellow solid, yield: 47% (140 mg); mp: 112–115 °C. FT-IR (KBr,  $\text{cm}^{-1}$ ): 3175, 3068, 2956, 1727, and 1691.  $^1\text{H}$  NMR ( $\text{CDCl}_3$ )  $\delta$ : 8.71(1H, s, H5-triazole), 8.62 (1H, s, C=CH), 7.67 (2H, m, H7, H8), 7.44 (2H, m, H5, H6), 5.33 (2H, m,  $\text{CH}_2$ ), 2.44 (1H, m, CH), 1.66 (2H, m,  $\text{CH}_2$ ), 1.45 (2H, m,  $\text{CH}_2$ ), 1.29 (4H, m,  $\text{CH}_2$ ,  $\text{CH}_2$ ), 0.90 (6H, t,  $J=7.3$  Hz,  $2\text{CH}_3$ ).  $^{13}\text{C}$  NMR ( $\text{CDCl}_3$ )  $\delta$ : 176.27, 155, 152.70, 143.52, 133.30, 132.88, 128.99, 125.62, 124.54, 122.96, 118.04, 116.76, 57.13, 45.06, 34.50, 20.59, and 13.97. Elemental analyses, found: C%, 64.97; H%, 6.45; N%, 11.54. Calc for  $\text{C}_{20}\text{H}_{23}\text{N}_3\text{O}_4$  (MW 369.41): C%, 65.03; H%, 6.28; N%, 11.37.

### Biological studies

The anticancer activity of the synthesised compounds was studied using high-efficiency biological screening methodology according to the Developmental Therapeutics Program (DTP) (Bethesda, MD), National Cancer Institute (NCI) (Bethesda, MD) and in the confirmatory diagnostic unit, VACSERA (Cairo, Egypt).

### Preliminary in vitro anticancer screening

Compounds (**8–17**) were submitted to the National Cancer Institute "NCI"; all the submitted compounds were selected for preliminary screening. The compounds were tested at a single dose of 10  $\mu\text{M}$  in the full NCI 60-cell panel.

### MTT assay for cell viability

The most active compounds (**8**, **9**, and **10**) were tested against MCF7 and DU-145 cells lines using MTT assay according to the standard protocol<sup>36</sup>.

### DNA-flow cytometry analysis

MCF7 cell lines ( $1 \times 10^6$  cell density) were subjected to 2.70  $\mu\text{M}$  of compound **8**, 10.86  $\mu\text{M}$  of **9**, 42.71  $\mu\text{M}$  of **10** and (0.002%) DMSO as a control for 24 h. In the same way, DU-145 cell lines ( $1 \times 10^6$  cell density) were subjected to 26  $\mu\text{M}$  of compound **8**, 59.34  $\mu\text{M}$  of **9**, and 79.27  $\mu\text{M}$  of **10** and (0.002%) DMSO as a control for 24 h. The cells were trypsinised for detachment, ice-cold PBS was used for washing and ice cold 70% EtOH was used for fixation. Afterwards, the cells remain at least 2 h at 4 °C in EtOH then centrifuged. Thereafter, PBS was used for washing of the cells and then Cycle TEST™ plus DNA Reagent Kit (ab139418\_Propidium Iodide Flow Cytometry Kit) was used for staining. FACS-Calibur flow cytometer and Cell Quest software (Becton Dickinson Biosciences, San Jose, CA) were used for determination of cell cycle distribution and analysis, respectively.

### Topoisomerase IIB inhibitory assay

This assay utilises human topoisomerase 2-beta (TOP2B) ELISA Kit. In brief, compounds **8–10** were evaluated using 10 folds serial concentration 0.01–100  $\mu\text{M}$  in a six-well plate for 24 h incubation at 37 °C and 5%  $\text{CO}_2$ . After treatment, cell suspension is diluted with PBS (pH 7.2–7.4), until cell concentration reached 10 million/ml. Then, store overnight at –20 °C. After two freeze–thaw cycles to break up the cell membranes, the cell lysates were centrifuged for 5 min at 2–8 °C; collected the supernatant. Cell lysates should be examined immediately or aliquoted and stored at –20 °C. One hundred microlitres of standard and sample per well was added and incubated for 2 h at 37 °C then 100  $\mu\text{L}$  of biotin-conjugated antibody specific for TOPIIB is added to each well. Incubate for 1 h at 37 °C, aspirated each well and wash. After washing, 100  $\mu\text{L}$  of avidin conjugated horseradish peroxidase (HRP) is added to each well; incubated for 1 h at 37 °C. After that 90  $\mu\text{L}$  of TMB Substrate is added to each well and incubated for 15–30 min at 37 °C; protected from light. Finally, 50  $\mu\text{L}$  of stop solution is added to each well and gently tapped the plate to ensure thorough mixing. The optical density of each well within 5 min, using a microplate reader was determined.

### Annexin V-FITC apoptosis assay

The most active compounds (**8**, **9**, and **10**) were assayed against HL-60 (TB) and MOLT-4 cell lines using Annexin V-FITC Apoptosis Detection Kit (BD Biosciences, Franklin Lakes, NJ) according to standard protocol<sup>36</sup>.

### Computational studies

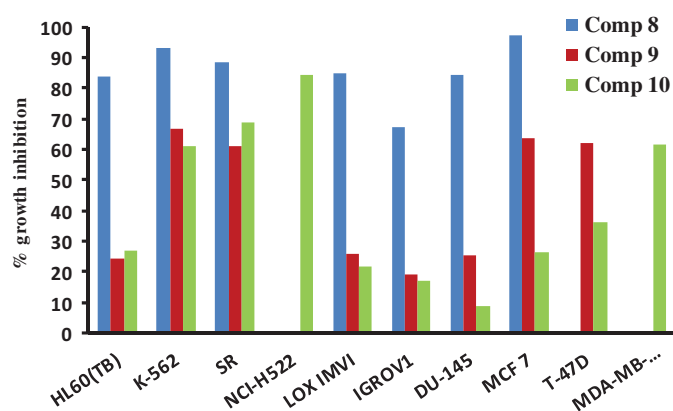
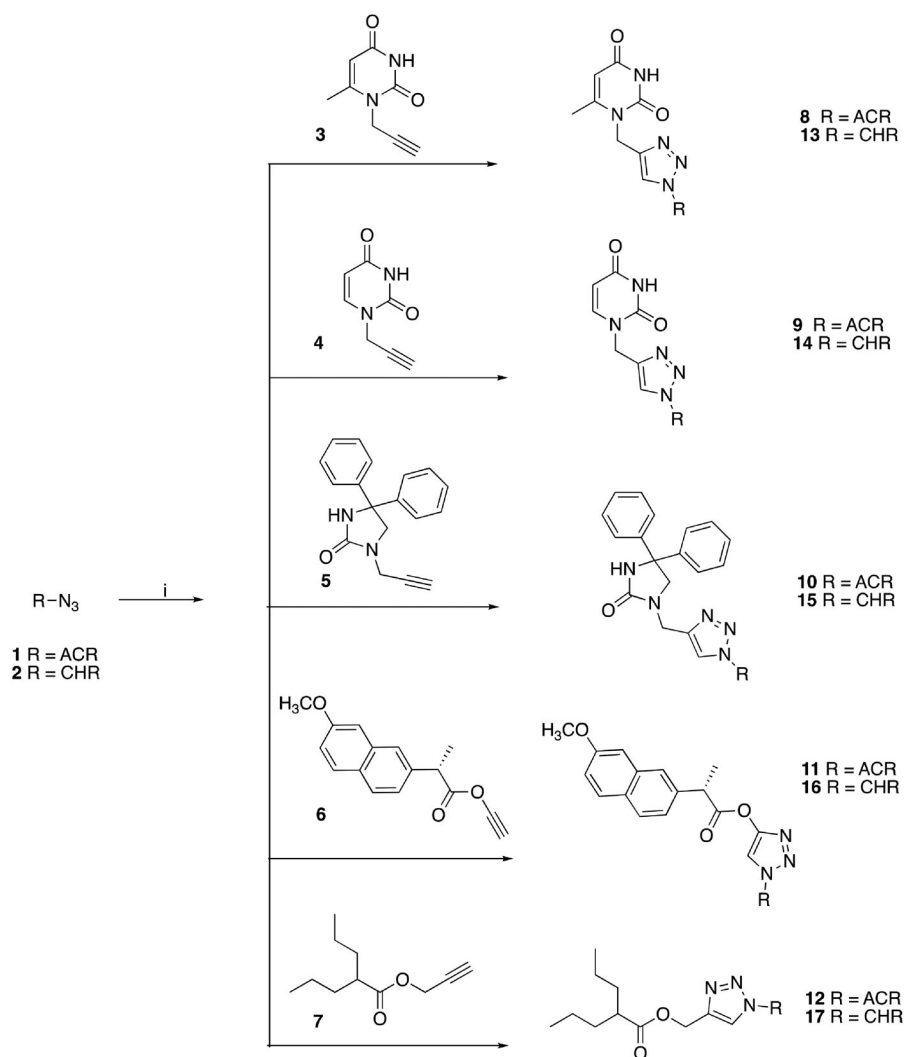
Molecular docking and molecular dynamics (MD) simulations were performed as previously described<sup>37–39</sup>. Briefly, the compounds were docked using the topoisomerase IIB crystal structure in complex with DNA (PDB ID: 4G0U)<sup>40</sup>, to generate PDB files of the topoisomerase IIB-ligand complexes, using molecular operating environment (MOE)<sup>41</sup> until a RMSD gradient of 0.01 kcal/mol/Å with the MMFF94 forcefield (ligands) and partial charges were automatically calculated. Docking was performed using the Alpha Triangle placement to determine the poses, refinement of the results was done using the MMFF94 forcefield and rescoring of the refined results using the London  $\Delta G$  scoring function was applied.

Molecular dynamics simulations were run on the topoisomerase IIB-ligand complexes with the PDB files first optimised with



**Table 1.** Yields, mp, and characteristic triazole  $^1\text{H}$  NMR of hybrid compounds.

Compound	Yield (%)	mp ( $^{\circ}\text{C}$ )	NMR triazole C-H	
			$^1\text{H}$ NMR	$^{13}\text{C}$ NMR
8	57	247–250	8.86	128.3
9	61	254–256	8.87	128.4
10	80	263–265	8.84	128.4
11	45	138–140	8.72	128.8
12	46	100–102	8.14	128.0
13	74	279–283	8.71	133.5
14	62	262–264	8.73	133.4
15	50	238–240	8.73	133.4
16	46	142–144	8.70	133.4
17	47	112–115	8.71	132.9

**Figure 3.** Comparative percent growth inhibition of 8–10 screened at single dose level.**Scheme 1.** Reagents and conditions: (i)  $\text{CuSO}_4 \cdot 5\text{H}_2\text{O}$ , sodium ascorbate, either  $\text{H}_2\text{O}/t\text{BuOH}$  (1:1 v/v) or  $\text{H}_2\text{O}/\text{THF}$  (1:1 v/v), 80 or  $60^{\circ}\text{C}$ , overnight (ACR = 9-acridinyl; CHR = 2H-chromen-2-one-3-yl).

protein preparation wizard in Maestro by assigning bond orders, adding hydrogen, and correcting incorrect bond types<sup>42,43</sup>. A default quick relaxation protocol was used to minimise the MD systems with the Desmond programme of Schrödinger<sup>44</sup>. The orthorhombic water box allowed for a 10 Å buffer region between protein atoms and box sides. Overlapping water molecules were deleted, and the systems were neutralised with  $\text{Na}^+$  ions and salt concentration of 0.15 M. Force-field parameters for the complexes

were assigned using the OPLS\_2005 forcefield, that is, a 200 ns molecular dynamic run in the NPT ensemble ( $T = 300\text{ K}$ ) at a constant pressure of 1 bar. Energy and trajectory atomic coordinate data were recorded at each 1.2 ns and a total of 1000 frames generated. Prime/MMGBAS<sup>45</sup>, available in Schrödinger Prime suite, was used to calculate the binding free energy of the ligands with topoisomerase IIB in complex with DNA.

$\Delta G(\text{bind}) = E_{\text{Complex}}(\text{minimised}) - (E_{\text{ligand}}(\text{minimised}) + E_{\text{receptor}}(\text{minimised}))$  (Table 2) Cytotoxicity profile and topoisomerase IIB inhibitory activity of compounds 8–10.

Mean  $\Delta G(\text{bind})$  values were calculated from each frame of the final 10 ns (50 frames) of the MD simulation (i.e. the equilibrated complex). The average generated  $\Delta G$  was from each energy minimised frame using the equation shown above.

## Results and discussion

### Chemistry

9-Azidoacridine (**1**) was prepared by nucleophilic substitution of 9-chloroacridine in the presence of sodium azide under dry conditions<sup>29</sup>, and 3-azido-2H-chromen-2-one **2** was prepared through cyclisation, hydrolysis, and diazotisation of 2-hydroxybenzaldehyde as previously described<sup>32</sup>. The propargyl derivatives (**3–7**) were prepared by conventional alkylation through the reaction of the active nucleophilic centres with propargyl bromide substrate<sup>32,33</sup>. The hybrid compounds (**8–17**) were synthesised by click reaction through cycloaddition of the respective azides (**1–2**) with propargyl derivatives (**3–7**) using copper (I) catalyst generated *in situ* via copper (II) sulphate reduction with sodium ascorbate (Scheme 1)<sup>46</sup>. For compounds **8–11** and **13–16**, the reaction was performed by heating at 80 °C in the presence of 10 equivalent of sodium ascorbate in aqueous *t*-BuOH (1:1 v/v), while for compounds **12** and **17** the reaction was performed in aqueous THF (1:1 v/v). The final hybrid compounds were obtained in moderate to good yields with structure confirmation by <sup>1</sup>H and <sup>13</sup>C NMR, which identified the characteristic triazole signal (Table 1).

### Biological evaluation

#### Preliminary *in vitro* anticancer screening

The hybrid compounds (**8–17**) were screened by the National Cancer Institute (NCI) (Bethesda, MD) in a primary anticancer assay in the full NCI-60 cell panel. The cell lines were derived from nine different cancer types: melanoma, leukaemia, colon, lung, CNS, renal, ovarian, breast, and prostate cancers. Compounds **11** and **12** having naproxen and valproic acid fragments in the acridine series as well all members of the set carrying the coumarin nucleus **13–17** showed either low or complete absence of cell growth inhibition against all cancer cell lines. However, compounds **8–10** of the acridine series having 6-methyluracil, uracil and phenytoin fragments displayed cell growth inhibition and selectivity against the different cell lines. Compound **8** displayed good to excellent cell growth inhibition against five types of cancer cell lines: leukaemia (K-562, HL-60 (TB), and SR), melanoma (LOX IMVI), ovarian (IGROV1), prostate (DU-145), and breast (MCF7) with percent growth inhibition of 83.7, 92.9, 88.6, 84.8, 67.0, 84.3, and 97.5, respectively. For compound **9**, cell growth inhibition ranging from 61.3 to 67.0% was observed against K-562 and SR, MCF7 and T-47D cell lines. Compound **10** showed comparable cell growth inhibition percent ranging from 60.8 to 68.6 against K-562, SR, and MDA-MB-468; however, it showed marked selectivity and the best inhibitory activity of 84.1% against NCI-H522 (non-small cell lung cancer). Figure 3 provides a comparison of the percent growth inhibition of the cell lines on treatment with compounds **8–10**.

#### MTT assay for cell viability

The cytotoxicity of compounds **8–10** against MCF-7 breast cancer and DU-145 prostate cancer cell lines was determined using the

Compound	Cytotoxicity IC <sub>50</sub> (μM ± SE)		Topoisomerase IIB IC <sub>50</sub> (μM)
	MCF7	DU-145	
<b>8</b>	2.70 (±0.08)	26.10 (±1.25)	0.52
<b>9</b>	10.86 (±0.61)	59.34 (±2.61)	0.86
<b>10</b>	42.71 (±1.54)	79.27 (±1.84)	2.56
Doxorubicin	2.06 (±0.04)	14.28 (±0.51)	0.83

MTT assay<sup>36,47</sup>. The compounds were all more cytotoxic in the MCF-7 cell line and in both cell lines the 6-methyluracil derivative (**8**) was more cytotoxic than the uracil derivative (**9**) with the bulkier phenytoin derivative (**10**) the least active (Table 2). Compound **8** displayed comparable cytotoxicity (IC<sub>50</sub> 2.70 ± 0.08 μM) with the standard doxorubicin (IC<sub>50</sub> 2.06 ± 0.04 μM), an anthracycline in clinical use as a wide spectrum antitumor agent, which exerts its action by intercalation between DNA double strands and blocks the topoisomerase II involved in the DNA replication process<sup>6</sup>.

#### Topoisomerase II B assay

The acridine compounds **8–10** were evaluated for inhibitory activity against MCF7 topoisomerase IIB and compounds **8** and **9** showed potent inhibitory activity with IC<sub>50</sub> of 0.52 μM and 0.86 μM respectively compared with doxorubicin IC<sub>50</sub> 0.83 μM, while the phenytoin derivative **10** was less active with IC<sub>50</sub> 2.56 μM (Table 2).

#### DNA-flow cytometry analysis

Cell cycle parameters were compared for MCF-7 and DU-145 cell lines incubated for 24 h with the compounds **8–10** at their IC<sub>50</sub> displayed in Table 2 and with vehicle (DMSO) as control. Cell cycle parameter for MCF-7 on exposure to compounds **8–10** showed induction of apoptosis as indicated by the increase in the percentage of apoptotic cells at the preG1 phase (24.4%, 16.3%, and 13.2% respectively compared with 2.3% for control) and decreased percentage of cells at G0/G1 phase (24.4%, 37.3%, and 43.5% respectively compared with 52.6% for control) and there was a concomitant increase in the cells at G2/M phase (48.3%, 39.8% and 15.3% compared with 10.1% for control) (Table 3).

Similarly, exposure of DU-145 to compounds **8–10** increased the preG phase cells population (12.9%, 6.7%, and 4.5% respectively compared with 1.9% for control), whereas G0/G1 cells significantly reduced (34.6%, 41.5%, and 42.9% respectively compared with 49.1% for control) accompanied by a notable increase in the cells at G2/M phase (39.6%, 29.1%, and 20.9% compared with 13.7% for control). The percentage of the cells in S-phase showed no significant difference. Therefore, it seems compounds **8–10** inhibit the cell proliferation through cell cycle arrest at the G2/M phase, which consequently induces cell death by apoptosis. In line with the cytotoxicity results, apoptosis was more pronounced in MCF-7 and DU-145 cell lines treated with compounds **8–10** than those treated with control (Table 3).

#### Annexin V-FITC apoptosis assay

To allow for a precise estimation of apoptotic incidence induced by compounds **8–10**, evaluation of the pro-apoptotic effect was performed by assay of the differential binding of the cells to propidium iodide (PI) and annexin V-FITC<sup>48</sup> that showed a notable effect on the percentage of apoptotic cells.

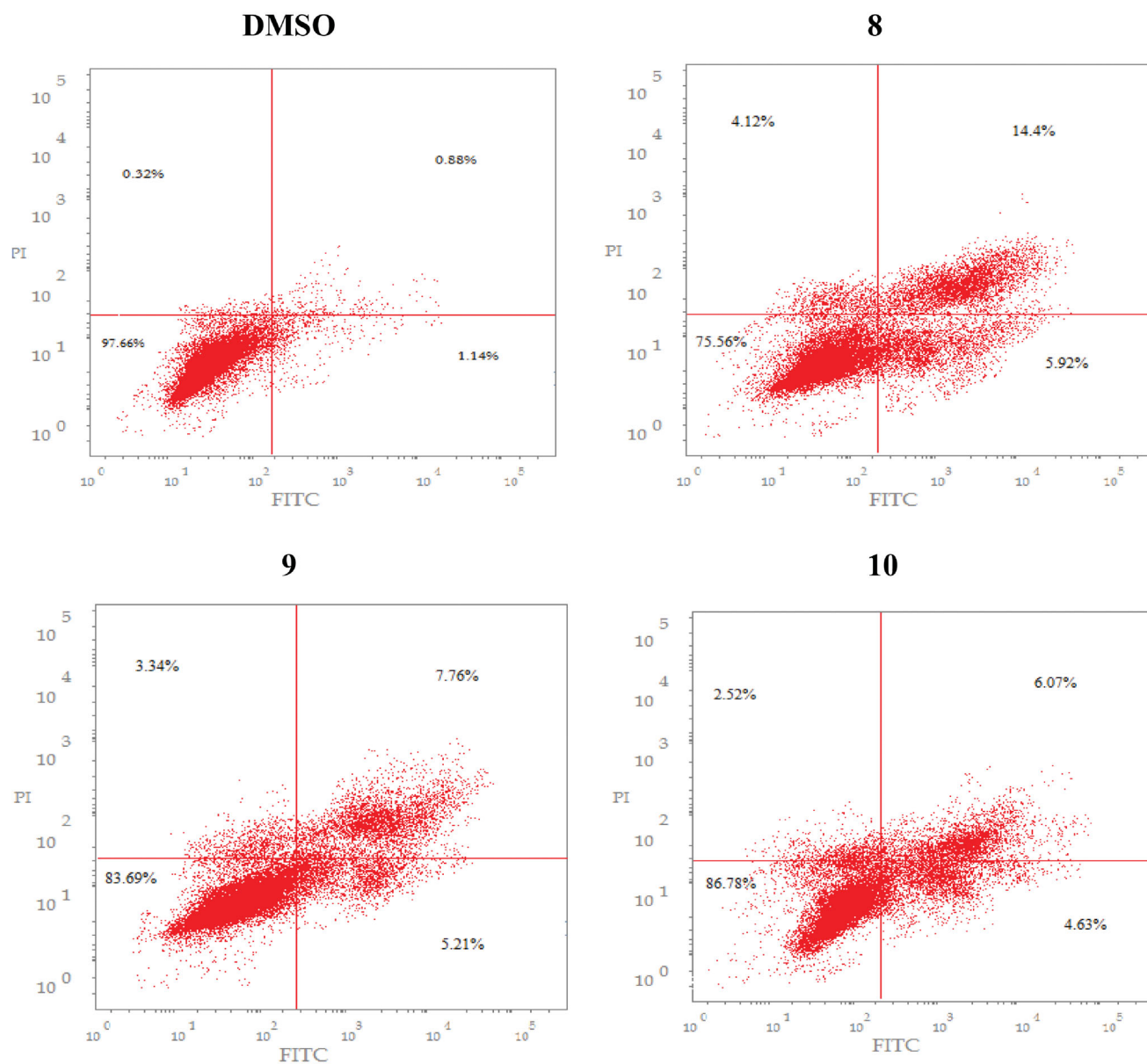


**Figure 4.** Effect of compounds **8–10** on the percentage of annexin V-FIT positive staining in MCF-7 cells on exposure for 24 h. The cells were treated with DMSO as control.

MCF-7 cells exposed to  $IC_{50}$  of compounds **8–10** revealed an increase in the percentage of annexin V-FITC positive apoptotic cells (UR+LR) 20.3% (10-fold) for **8**, 13% (6.4-fold) for **9**, and 10.7% (5.3-fold) for **10** compared with vehicle control (2.0%) (Figure 4). DU-145 cells showed a rise in the percent of annexin V-FITC positive apoptotic cells (UR+LR) 10.2% (sixfold) for **8**, 4.3% (5.9-fold) for **9**, and 3.6% (2 fold) for **10** compared with vehicle control (1.7%) (Figure 5). These results showed that the antiproliferative effect of compounds **8**, **9**, and **10** is due to their strong pro-apoptotic activity and further confirmed our findings on the sensitivity of the assayed cell lines to the tested compounds.

#### Computational studies

Computational studies of acridine hybrid derivatives **8–10** were performed using human topoisomerase IIB in complex with DNA and amsacrine (PDB ID: 4G0U)<sup>40</sup>. The topoisomerase IIB–ligand complexes were prepared by computational docking of **8**, **9**, and

**Table 3.** Cell cycle perturbation of MCF7 and DU-145 cell lines treated with **8**, **9**, and **10** ligands and in the presence of control (DMSO).

Compound	Cell line	%G1	%S	%G2/M	%Pre-G1
<b>8</b>	MCF7	24.4	27.3	48.3	24.4
<b>9</b>	MCF7	37.3	22.9	39.8	16.3
<b>10</b>	MCF7	43.5	41.2	15.3	13.2
DMSO	MCF7	52.6	37.3	10.1	2.3
<b>8</b>	DU-145	34.6	25.8	39.6	12.9
<b>9</b>	DU-145	41.5	29.4	29.1	6.7
<b>10</b>	DU-145	42.9	36.2	20.9	4.5
DMSO	MCF7	49.1	37.2	13.7	1.9

**10** the using MOE software<sup>41</sup> and then subject to 200 ns MD simulations using the Desmond programme of Maestro<sup>44</sup>.

The 6-methyluracil ring on compound **8** is positioned between nucleic acid bases guanine (DG13) and cytidine (DC14) and forms a  $\pi$ - $\pi$  interaction with DG13 and a H-bonding interaction between the 6-methyluracil NH and the carbonyl oxygen of the cytidine ring

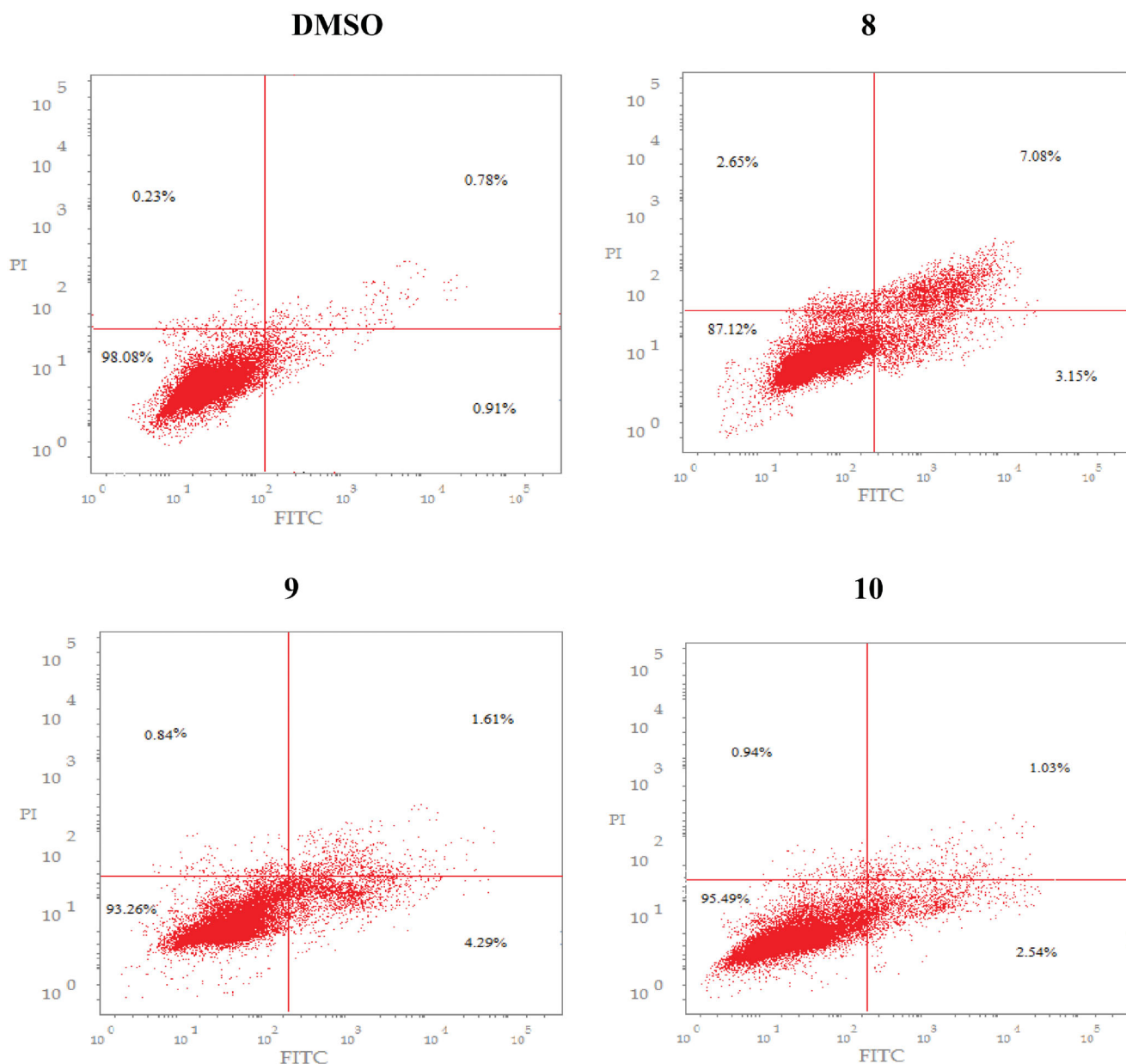


**Figure 5.** Effect of compounds **8–10** on the percentage of annexin V-FITC positive staining in DU-145 cells on exposure for 24 h. The cells were treated with DMSO as control.

of DC14 (Figure 6(A)). The triazole ring of compound **8** also forms an H-bonding interaction between one of the triazole N atoms and the guanine NH of DG13, while the acridine ring is positioned parallel to the thymine ring of DT9 allowing formation of a  $\pi$ - $\pi$  interaction. The complex is also stabilised by van der Waals interactions and hydrogen bonds with Val760, Gln778, Met781, Met782, Val785, Lys814, Ala816, Ala817, Pro819, and Ile822 (Figure 7(A)), with a binding affinity ( $\Delta G$ ) of  $-49.6 \pm 4$  kcal/mol.

In the case of compound **9**, the anthracene is positioned closer to the major groove but between the nucleic acid bases adenine (DA12) and guanine (DG13) and forms a  $\pi$ - $\pi$  interaction with DG13, while the uracil carbonyl oxygen forms a H-bonding interaction with DG13 and the triazole is positioned to form a  $\pi$ - $\pi$  interaction with DT9 and also forms a water mediated H-bonding interaction between one of the triazole N atoms and the phosphate backbone of DT9 (Figure 6(B)). Although not as optimally positioned as compound **8**, the uracil of compound **9** sits in a pocket composed of Glu417, Arg503, Gly504, Lys505, Asp561, and

Ile565 stabilised by van der Waals interactions and hydrogen bonds, while the anthracene forms additional interactions with Gln778, Ala779, and Met782, resulting in a binding affinity ( $\Delta G$ ) of  $-35.9 \pm 3$  kcal/mol (Figure 7(B)).

The acridine moiety of the phenytoin derivative **10** is also positioned between the nucleic acid bases DA12 and DG13 forming a  $\pi$ - $\pi$  interaction with DT12 and an edge to face  $\pi$ - $\pi$  interaction with DC13 (Figure 6(C)). The phenytoin forms H-bonding interactions between one of the carbonyl oxygens and DG13 NH<sub>2</sub> and DC14 cytidine ring, and the triazole ring forms an aryl-cation interaction with DG13. As seen with compound **9**, the anthracene moiety of compound **10** sits in a pocket composed of Gln778, Ala779, Met781, Met782, and Met782 (Figure 7(C)). The phenytoin derivative (**10**) has an improved binding affinity ( $\Delta G$ ) of  $-67 \pm 5$  kcal/mol compared with the 6-methyluracil (**8**) and uracil (**9**) derivatives, which can be explained by the positioning of the bulky phenytoin group in a much wider pocket perpendicular to the acridine moiety, but away from the binding site, to minimise steric clashes (Figure 8).



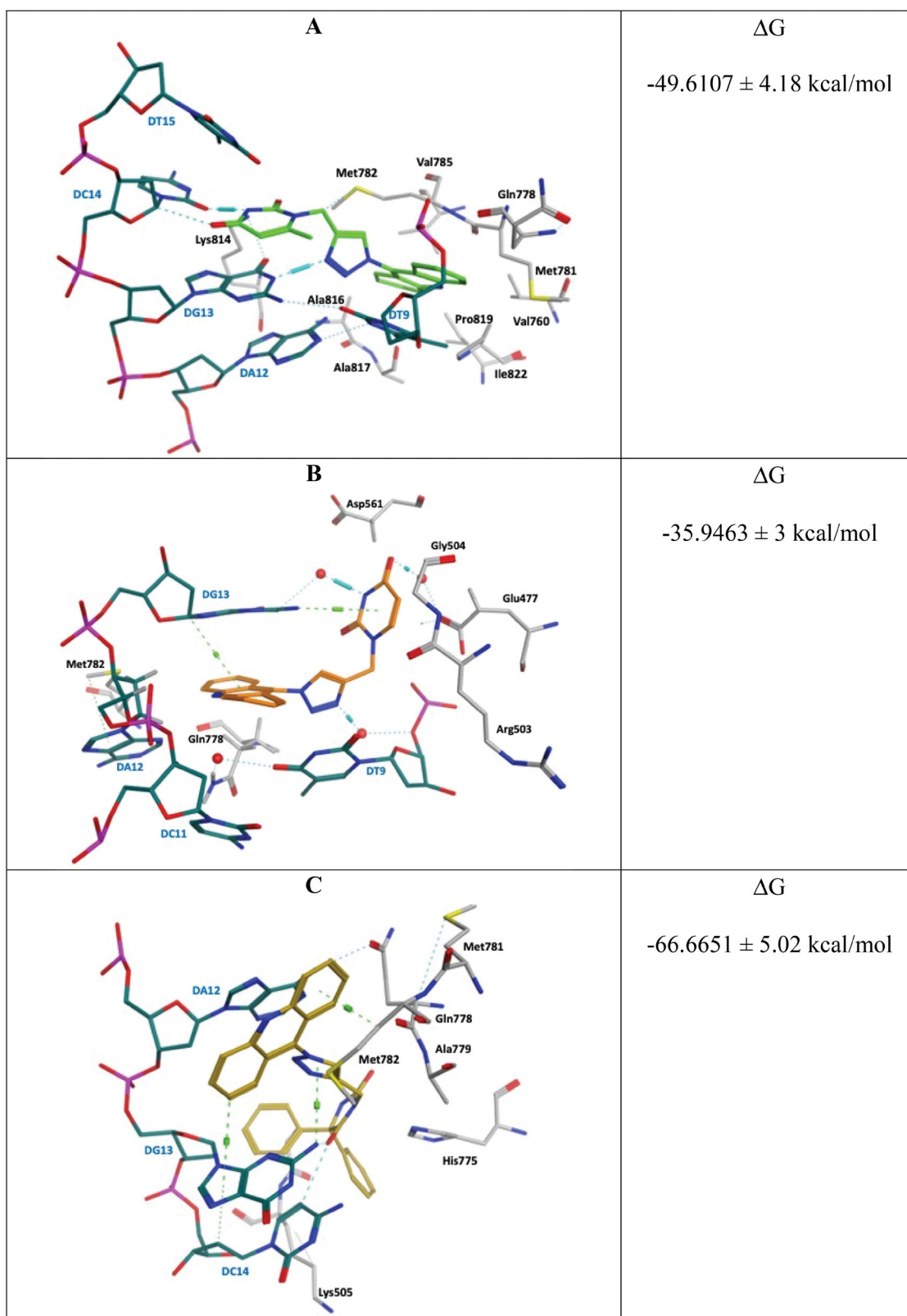


**Figure 6.** 3D representation of the binding mode (A) compound **8** (green), (B) compound **9** (orange), and (C) compound **10** (gold). DNA structure (teal), protein (grey), and water molecules (red spheres).

## Conclusions

The designed three component hybridised acridine and coumarin derivatives were synthesised and evaluated for their *in vitro* cancer

cell growth inhibition activity. Among the acridine series compounds **8**, **9**, and **10** showed significant growth inhibition (61–97%) against six cancer cell lines. DNA interaction and topoisomerase inhibition properties of the planar tricyclic acridine ring

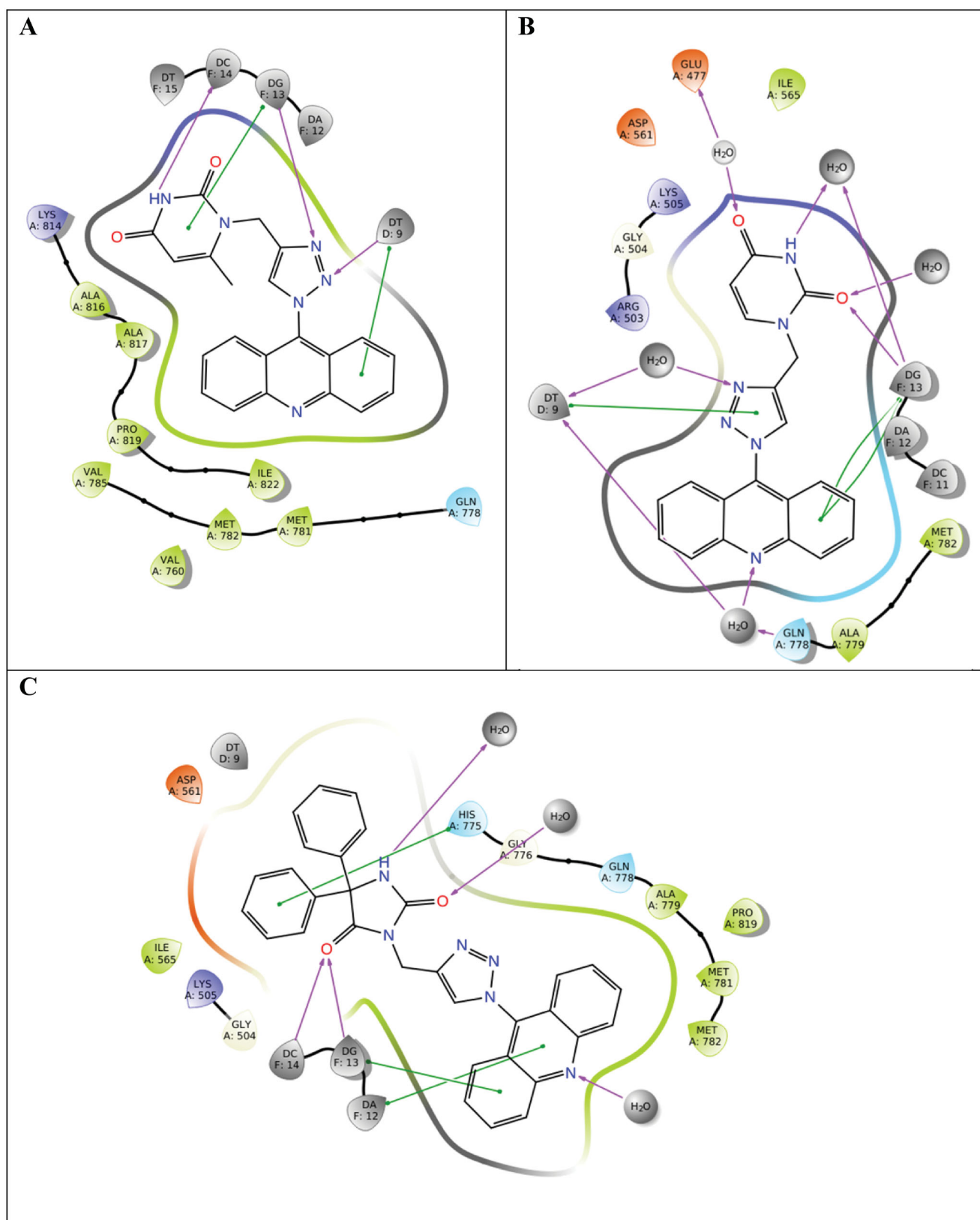


**Figure 7.** Ligand interactions of final frame after 200ns simulation of the topoisomerase IIB-ligand complexes of (A) compound 8 (B) compound 9 and (C) compound 10.

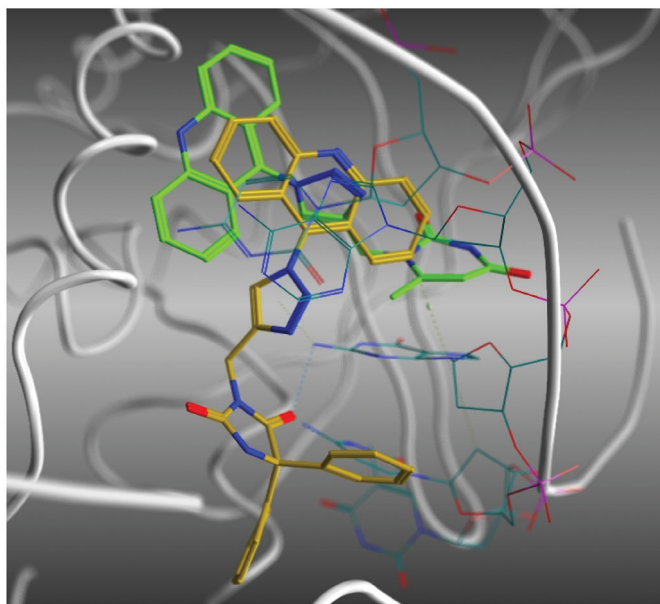


**Figure 8.** Positioning of the bulky phenytoin moiety of derivative **10** (gold) away from the binding site in comparison with the 6-methyluracil derivative **8** (green) in topoisomerase IIB.

inducing cell apoptosis were demonstrated by flow cytometry and pro-apoptotic cell accumulation via the differential binding of the cells to annexin V-FITC and PI of MCF7 and DU-145 cell lines. Compounds **8**, **9**, and **10** showed cell growth inhibition at the micromolar level. MCF7 and DU-145 exposed to the most active compound **8** revealed  $IC_{50}$  values of 2.7 and 26.1  $\mu\text{M}$  respectively, which are comparable with the reference doxorubicin  $IC_{50}$  values of 2.0 and 14.2  $\mu\text{M}$ , respectively. DNA topoisomerase type IIB is involved in control of DNA replication and chromosome segregation during the normal cell cycle. Two new compounds **8** and **9** showed topoisomerase IIB inhibition potential with  $IC_{50}$  of 0.52  $\mu\text{M}$  and 0.86  $\mu\text{M}$  respectively in comparison to the reference drug doxorubicin  $IC_{50}$  of 0.83  $\mu\text{M}$ . Computational studies illustrated the optimal positioning of the 6-methyluracil derivative **8** for intercalation with the DNA bases DG13, DC14, and DT9 with the 6-methyluracil and anthracene moieties respectively with additional protein–ligand interactions to stabilise the ligand in the binding site. The uracil derivative **9** is orientated in the opposite position with the anthracene positioned to intercalate with DG13 and in this case the triazole is positioned above DT9. The anthracene of the bulky phenytoin is positioned between DA12 and DG13, the phenytoin does not interact with DT9 and owing to steric limitations is extended away from the binding site with more limited protein–ligand interactions. The difference in binding interactions determined by the ligand conformation resulted in variances in cell growth inhibition and cytotoxic activity that can explain the depletion of anticancer activity of the other members of the prepared series **11–17**. Owing to the promising results for the acridine derivatives with substituted pyrimidines, this pharmacophore can be considered as a lead for optimisation.

### Acknowledgements

Molecular dynamics simulations were undertaken using the super-computing facilities at Cardiff University operated by Advanced Research Computing at Cardiff (ARCCA) on behalf of the Cardiff Supercomputing Facility and the HPC Wales and Supercomputing Wales (SCW) projects.

### Disclosure statement

The authors declare that they have no known competing financial interests or personal relationships that could have appeared to influence the work reported in this paper.

### Funding

The authors acknowledge support of the latter, which is part-funded by the European Regional Development Fund (ERDF) via the Welsh Government.

### References

- Mokdad AH, Dwyer-Lindgren L, Fitzmaurice C, et al. Trends and patterns of disparities in cancer mortality among us counties, 1980–2014. *JAMA* 2017;317:388–406.
- Siegel RL, Miller KD, Jemal A. Cancer statistics, 2019. *CA Cancer J Clin* 2019;69:7–34.
- Fortin S, Bérubé G. Advances in the development of hybrid anticancer drugs. *Expert Opin Drug Discov* 2013;8:1029–47.
- Belmont P, Dorange I. Acridine/acridone: a simple scaffold with a wide range of application in oncology. *Expert Opin Ther Pat* 2008;18:1211–24.
- Sayed M, Krishnamurthy B, Pal H. Unraveling multiple binding modes of acridine orange to DNA using a multispectroscopic approach. *Phys Chem Chem Phys* 2016;18:24642–53.
- Pogorelnik B, Perdih A, Solmajer T. Recent developments of DNA poisons—human DNA topoisomerase II $\alpha$  inhibitors—as anticancer agents. *Curr Pharm Des* 2013;19:2474–88.
- Cholewiński G, Dzierzbicka K, Kołodziejczyk AM. Natural and synthetic acridines/acridones as antitumor agents: their biological activities and methods of synthesis. *Pharmacol Rep* 2011;63:305–36.
- Bridewell DJ, Finlay GJ, Baguley BC. Mechanism of cytotoxicity of N-[2-(dimethylamino)ethyl] acridine-4-carboxamide and of its 7-chloro derivative: the roles of topoisomerases I and II. *Cancer Chemother Pharmacol* 1999;43:302–8.
- Demeunynck M. Antitumour acridines. *Expert Opin Ther Pat* 2004;14:55–70.
- Gensicka-Kowalewska M, Cholewiński G, Dzierzbicka K. Recent developments in the synthesis and biological activity of acridine/acridone analogues. *RSC Adv* 2017;7:15776–804.
- Venugopala KN, Rashmi V, Odhav B. Review on natural coumarin lead compounds for their pharmacological activity. *BioMed Res Int* 2013;2013:963248.
- Wu X-Q, Huang C, Jia Y-M, et al. Novel coumarin-dihydropyrazole thio-ethanone derivatives: design, synthesis and anticancer activity. *Eur J Med Chem* 2014;74:717–25.
- Fong W-F, Shen X-L, Globisch C, et al. Methoxylation of 3',4'-aromatic side chains improves P-glycoprotein inhibitory and multidrug resistance reversal activities of 7,8-pyranocoumarin against cancer cells. *Bioorg Med Chem* 2008;16:3694–703.
- Agalave SG, Maujan SR, Pore VS. Click chemistry: 1,2,3-triazoles as pharmacophores. *Chem Asian J* 2011;6:2696–718.
- Thirumurugan P, Matosiuk D, Jozwiak K. Click chemistry for drug development and diverse chemical-biology applications. *Chem Rev* 2013;113:4905–79.
- Mackay HJ, Hill M, Twelves C, et al. A phase I/II study of oral uracil/tegafur (UFT), leucovorin and irinotecan in patients with advanced colorectal cancer. *Ann Oncol* 2003;14:1264–9.

17. van Staveren MC, Opdam F, Guchelaar HJ, et al. Influence of metastatic disease on the usefulness of uracil pharmacokinetics as a screening tool for DPD activity in colorectal cancer patients. *Cancer Chemother Pharmacol* 2015;76:47–52.
18. Keppel Hesselink JM, Kopsky DJ. Phenytoin: 80 years young, from epilepsy to breast cancer, a remarkable molecule with multiple modes of action. *J Neurol* 2017;264:1617–21.
19. Yang M, Kozminski DJ, Wold LA, et al. Therapeutic potential for phenytoin: targeting Na(v)1.5 sodium channels to reduce migration and invasion in metastatic breast cancer. *Breast Cancer Res Treat* 2012;134:603–15.
20. Razmaraii N, Babaei H, Mohajjel Nayebi A, et al. Cardioprotective effect of phenytoin on doxorubicin-induced cardiac toxicity in a rat model. *J Cardiovasc Pharmacol* 2016; 67:237–45.
21. Michaelis M, Doerr WH, Cinatl J Jr. Valproic acid as anti-cancer drug. *Curr Pharm Des* 2007;13:3378–93.
22. Göttlicher M, Minucci S, Zhu P, et al. Valproic acid defines a novel class of HDAC inhibitors inducing differentiation of transformed cells. *EMBO J* 2001;20:6969–78.
23. Han M, Küçükgülmez ŞG. Anticancer and antimicrobial activities of naproxen and naproxen derivatives. *Mini Rev Med Chem* 2020;20:1300–10.
24. Kim MS, Kim JE, Lim DY, et al. Naproxen induces cell-cycle arrest and apoptosis in human urinary bladder cancer cell lines and chemically induced cancers by targeting PI3K. *Cancer Prev Res* 2014;7:236–45.
25. Dheer D, Singh V, Shankar R. Medicinal attributes of 1,2,3-triazoles: current developments. *Bioorg Chem* 2017;71:30–54.
26. Nagarjuna G, Yurt S, Jadhav KG, Venkataraman D. Impact of pendant 1, 2, 3-triazole on the synthesis and properties of thiophene-based polymers. *Macromolecules* 2010;43: 8045–50.
27. Bock VD, Hiemstra H, Van Maarseveen JH. Cu-catalyzed alkyne-azide “click” cycloadditions from a mechanistic and synthetic perspective. *Eur J Org Chem* 2006;2006:51–68.
28. Bräse S, Gil C, Knepper K, Zimmermann V. Organic azides: an exploding diversity of a unique class of compounds. *Angew Chem Int Ed Engl* 2005;44:5188–240.
29. Taherpour AA, Kvaskoff D, Bernhardt PV, Wentrup C. 9-Azidoacridine and 9-acridinyl nitrene. *J Phys Org Chem* 2010; 23:382–9.
30. Meldal M, Tornøe CW. Cu-catalyzed azide-alkyne cycloaddition. *Chem Rev* 2008;108:2952–3015.
31. Kudale AA, Kendall J, Warford CC, et al. Hydrolysis-free synthesis of 3-aminocoumarins. *Tetrahedron Lett* 2007;48: 5077–80.
32. Al-Nuzal SMD. New derivatives of 3-substituted 5, 5-diphenyl-2, 4-imidazolidinedione as anticonvulsant and anti-epileptic candidates. *J Appl Chem* 2014;3:1319–26.
33. Krim J, Taourirte M, Engels JW. Synthesis of 1,4-disubstituted mono and bis-triazolocarbo-acyclonucleoside analogues of 9-(4-hydroxybutyl)guanine by Cu(I)-catalyzed click azide-alkyne cycloaddition. *Molecules* 2011;17:179–90.
34. Krivonogov V, Tolstikov G, Murinov YI, et al. Alkylation of 6-methyluracil and its derivatives. *Russ J Appl Chem* 1997;70: 301–6.
35. Tesak JL. Study of click chemistry: working towards ‘clicking’ a non-steroidal anti-inflammatory to an apoptosis inhibitor Q-VD-OPH [dissertation]. Miami University; 2012.
36. Ragab FAF, Abou-Seri SM, Abdel-Aziz SA, et al. Design, synthesis and anticancer activity of new monastrol analogues bearing 1,3,4-oxadiazole moiety. *Eur J Med Chem* 2017;138: 140–51.
37. Hofny HA, Mohamed MFA, Gomaa HAM, et al. Design, synthesis, and antibacterial evaluation of new quinoline-1,3,4-oxadiazole and quinoline-1,2,4-triazole hybrids as potential inhibitors of DNA gyrase and topoisomerase IV. *Bioorg Chem* 2021;112:104920.
38. Pasqualetto G, Schepelmann M, Varricchio C, et al. Computational studies towards the identification of novel rhodopsin-binding compounds as chemical chaperones for misfolded opsins. *Molecules* 2020;25:4904.
39. Kishk SM, Kishk RM, Yassen ASA, et al. Molecular insights into human transmembrane protease serine-2 (TMP22) inhibitors against SARS-CoV2: homology modelling, molecular dynamics, and docking studies. *Molecules* 2020;25:5007.
40. Wu C-C, Li Y-C, Wang Y-R, et al. On the structural basis and design guidelines for type II topoisomerase-targeting anti-cancer drugs. *Nucleic Acids Res* 2013;41:10630–40.
41. Molecular Operating Environment (MOE). Chemical Computing Group Ulc; 2020. Available from: <https://www.chemcomp.com/products.htm>.
42. Protein Preparation Wizard; 2021. Available from: <https://www.Schrodinger.Com/products/protein-preparation-wizard>.
43. Sastry GM, Adzhigirey M, Day T, et al. Protein and ligand preparation: parameters, protocols, and influence on virtual screening enrichments. *J Comput Aided Mol Des* 2013;27:221–34.
44. Schrödinger release 2020-1. New York (NY)/New York (NY). Desmond Molecular Dynamics System, D. E. Shaw Research/ Maestro-Desmond Interoperability Tools, Schrödinger; 2020. Available from: <https://www.schrodinger.com/products/desmond>.
45. Hou T, Wang J, Li Y, Wang W. Assessing the performance of the MM/PBSA and MM/GBSA methods. 1. The accuracy of binding free energy calculations based on molecular dynamics simulations. *J Chem Informat Model* 2011;51:69–82.
46. Himo F, Lovell T, Hilgraf R, et al. Copper(I)-catalyzed synthesis of azoles. DFT study predicts unprecedented reactivity and intermediates. *J Am Chem Soc* 2005;127:210–6.
47. Mosmann T. Rapid colorimetric assay for cellular growth and survival: application to proliferation and cytotoxicity assays. *J Immunol Methods* 1983;65:55–63.
48. Wlodkowic D, Telford W, Skommer J, Darzynkiewicz Z. Chapter 4: Apoptosis and beyond: cytometry in studies of programmed cell death. In: Darzynkiewicz Z, Holden E, Orfao A, Telford W, Wlodkowic D, ed. *Methods in cell biology*. London: Elsevier; 2011.